THE JOURNAL OF PHYSICAL CHEMISTRY B

Article

pubs.acs.org/JPCB

Probing Structure and Dynamics of Bulk and Confined Crude Oils by Multiscale NMR Spectroscopy, Diffusometry, and Relaxometry

Jean-Pierre Korb,* Alain Louis-Joseph, and Lyès Benamsili

Physique de la Matière Condensée, Ecole Polytechnique-CNRS, 91128 Palaiseau, France

ABSTRACT: We propose using a set of noninvasive multiscale NMR techniques for probing the structure and dynamics of bulk and confined crude oils with and without asphaltene. High-field 1D ^{1}H and ^{13}C NMR spectroscopies evidence the proton species and the amount of asphaltene and give an average chain length for the hydrocarbon aliphatic chains. Two-dimensional ^{1}H diffusion-ordered NMR spectroscopy (DOSY) spectra allow us to identify two populations of hydrocarbons characterized by two distributions of translational diffusion coefficients in the presence of asphaltene and a single one without asphaltene. A detailed analysis of the distributions of longitudinal, T_1, relaxation times measured at different magnetic fields is proposed in terms of highly skewed bimodal (or monomodal) log-normal distributions, confirming the two environments in the presence of asphaltene and a single one without asphaltene. We show that these distributions are similar to the gas and gel permeation chromatography distributions, thus showing a connection of the hydrocarbon dynamics with their chain lengths. The remarkable observed features of the nuclear magnetic relaxation dispersion (NMRD) profiles of $<1/T_1>$ for bulk and confined crude oils with and without asphaltene are interpreted with an original relaxation model of intermittent surface dynamics of proton species at the proximity of asphaltene nanoaggregates and bulk dynamics in between clusters of these nanoaggregates. This allows us to probe the 2D translational diffusion correlation time and the time of residence of hydrocarbons in the proximity of the asphaltene nanoaggregates. Provided that the diffusion of the hydrocarbons close to the asphaltene nanoaggregates is three times smaller than the bulk diffusion, as the DOSY experiments show, this time of residence gives an average radius of exploration for the 2D hydrocarbon diffusion, $r_{2D} \approx 3.9$ nm, of the same order of magnitude as the aggregate sizes found by J. Eyssautier with SAXS and SANS in asphaltene solutions and by O. C. Mullins with the observation of gravitational gradients of asphaltenes in oilfield reservoirs.

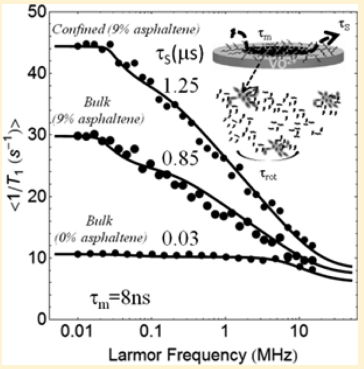

I. INTRODUCTION

Crude oils are among the most complex existing natural fluids. They contain several thousands of chemical species including hydrocarbons that come with a large range of structures and molecular sizes. Several analytical techniques are usually required for the analysis of their complex chemical structures such as chromatography[1] and mass spectroscopy.[2] However, standard gas chromatography (GC) is limited to molecules with fewer than 30 carbons, while gel permeation chromatography (GPC) extends the analysis of much larger carbon chain lengths. Mass spectroscopy is an invasive technique that suffers from the difficulty of ionizing all of the different classes of molecules. This makes the quantitative analysis difficult. Another difficulty comes from the presence of asphaltene molecules that are responsible for plugging the pores of reservoirs and catalytic networks.[3] These polar molecules represent a solubility class defined as the *n*-alkane insoluble and toluene-soluble fraction of petroleum. They are composed of a high degree of polynuclear aromatic rings that have alkyl side chains and incorporate heteroatoms (such as O, N, and S). The tendency of asphaltenes to self-aggregate distinguishes them from other oil constituents. For instance, asphaltene aggregation is the cause of complex effects occurring in oil viscosity, adsorption at solid surfaces, precipitation, fluid rheology, and emulsion stability. Recent X-ray (SAXS) and neutron (SANS) small-angle scattering studies[4] in asphaltene solutions have shown that asphaltenes form discoidal nanoaggregates of total radius 3.2 nm with 30% polydispersity and a height of 6.7 Å and a radius of gyration ∼7 nm for the macroaggregates. J. Eyssautier has also shown that the SAXS spectra are comparable for asphaltene diluted in maltenes, and the radii of gyration of the macro aggregates become smaller around 4 nm and decrease at high temperature.[5] However, the size of the asphaltene macroaggregates can vary depending on the type of oil and asphaltenes and method used to measure them. For instance, O. C. Mullins has recently shown that the radius of such macroaggregates was found to be 2.6 nm for oils in reservoirs.[6] Several attempts were made to study the structure of crude oils by high-field NMR spectroscopy.[7−10] However, the complete assignments of the different peaks become quite impossible for such a complex fluid. Low-field 1D and 2D NMR relaxometry and diffusometry were successfully used for studying the molecular dynamics of petroleum fluids.[11−13] These methods are even very useful in logging applications.[14] Nuclear magnetic relaxation dispersion (NMRD) studies of spin−lattice relaxation time T_1 at variable

Received: December 4, 2012
Revised: March 18, 2013
Published: May 20, 2013

magnetic fields[15] offer a variety of opportunities for characterizing the molecular dynamics of water and oils in confined environments such as calibrated glass beads,[16] granular packings,[17,18] and petroleum rocks.[19] This technique has recently probed the reality of asphaltene aggregation in crude oils.[20] However, a quantitative analysis of the NMRD dispersion profiles in the presence or absence of asphaltene has still not been proposed.

Here we propose multiscale 1D and 2D NMR spectroscopy, diffusometry, and relaxometry for probing the structure and dynamics of bulk and confined crude oils with and without asphaltene. High-field 1D ^{1}H and ^{13}C NMR spectra evidence the proton species, give an average chain length for the hydrocarbon aliphatic chains, and confirm the amount of asphaltene. The comparison of ^{1}H diffusion ordered spectroscopy (DOSY) spectra,[21,22] with and without asphaltene, allows us to identify two populations of hydrocarbons characterized by two distributions of translational diffusion coefficients. Standard GC and GPC report a highly skewed distribution of moles of hydrocarbon chain lengths that we fit by a probability density function (pdf) built as a bimodal log-normal distribution. We show that the shapes of the distribution of longitudinal relaxation times, T_1, at low magnetic fields obtained by an inverse Laplace transform method (ILT)[23,24] on bulk crude oil with asphaltene, at low fields, are similar to the GC and GPC distributions. This shows that the molecular dynamics of the hydrocarbon chains, sensed by the T_1 measurements, is correlated to the chain lengths. However, our primary measurement for probing the proton species dynamics is the magnetic field dependence or relaxation dispersion of the proton spin−lattice relaxation rate constant $1/T_1$ (NMRD[15]). We propose a detailed analysis of the distribution of longitudinal relaxation time, T_1, measured at variable magnetic fields, confirming the bimodal log-normal distribution in the presence of asphaltene and a monomodal log-normal distribution in the absence of asphaltene. The remarkable features of the NMRD profiles of $1/T_1$ for bulk and confined crude oils, with and without asphaltene, support an original interpretation in terms of coupled solid/liquid relaxation and surface diffusion in the proximity of asphaltene nanoaggregates, within clusters of such nanoaggregates (macroaggregates) and in between these macroaggregates. This allows probing the 2D translational diffusion correlation time as well as the time of residence of the hydrocarbons at the proximity of asphaltene nanoaggregates. Provided that the diffusion of the hydrocarbons close to the surface of asphaltene nanoaggregates is three times less than the bulk diffusion, as the DOSY experiments show, this time of residence measured at 25 °C, gives an average radius of 2D diffusion exploration $r_{2D} \approx 3.9$ nm of the same order of magnitude of the sizes of asphaltene aggregates previously found by SAXS and SANS in asphaltene solutions[4] and with the cluster sizes recently obtained, at higher temperatures, by the observations of gravitational gradients of asphaltenes in oilfield reservoirs.[6]

II. EXPERIMENTAL SECTION AND DATA TREATMENT

1. Materials. The crude oil used in this study was supplied by Total (EP, France). All of the samples were exposed to the air, so they lost their volatile components. In consequence, they were all in stable configurations. The standard petroleum industry protocol was used for analyzing the studied crude oil. The SARA analysis reveals a composition of saturates 40.3% (wt), aromatics 44.0% (wt), resins 6.7% (wt), and asphaltenes 9.0% (wt), respectively. Four different kinds of samples were prepared.

Sample 1: This is a bulk crude oil where the analysis reveals 9% (weight) of asphaltene, a viscosity η = 25 cP, and a density ρ_{oil} = 0.85 g/cm^3 at 25 °C.

Sample 2: This is a bulk sample prepared with the usual microdistillation to remove the weak fraction of oil. The distillation residue is precipitated in *n*-pentane. The latter is evaporated away to retrieve the remaining crude oil without asphaltene. The final evaporation of *n*-pentane under nitrogen flux, after filtration of asphaltenes, has been controlled by successive weights up to stabilization of the mass of maltenes. The GC analysis of the desasphaltene residue, after this evaporation under nitrogen flux and the different operations, evidences that the residual *n*-pentane represents <1% (wt) of the distilled desasphalted residue. Because of the low quantity obtained for sample 2, it has not been possible to evaluate its viscosity. However, the measurement of $1/T_1 \propto \eta$, at high frequency, shows clearly that its viscosity is lower than the one of sample 1.

Sample 3: This is the same crude oil as that used in sample 1 but confined within the pores of a well-characterized sandstone rock. The average porosity and permeability are 22.75% and 2.5D, respectively. The rock contains <5% of clays, 0.13% of iron (Fe), and a few ppm of Mn. X-ray μCT shows that there is a homogeneous pore size distribution centered on 25 μm.[25]

Sample 4: This is a reformed bulk sample prepared by a recombination of oil from the non-deasphalted residue of sample 1 (reference) after the first step of microdistillation and adding the initial non-deasphalted distillate of sample 1.

The different samples were placed in 10 or 5 mm sealed NMR tubes and measured at atmospheric pressure and controlled room temperature.

2. 1D and 2D NMR Spectroscopy. *1D ^{1}H NMR Spectrum.* The 1D ^{1}H NMR spectrum of crude oil with 9% asphaltene (sample 1) performed on a Bruker Avance II 300 micro bay with a probe ^{1}H with Z gradient coil is shown in Figure 1a. A small amount of perdeuterated toluene solvent has been added to lock the spectrometer for field stability and homogeneity. The small single peak at 2.2 and doublet at 7.3 ppm are unambiguously due to the few protonated toluenes. We have measured the 1D ^{1}H NMR spectrum without adding the toluene and observed the weak and large peaks of other aromatic protons. The spectral features between 0.5 and 1.9 ppm come from the aliphatic protons. We report in the inset of Figure 1a a zoom on the aliphatic part of the spectrum with the relative ratio of intensities of the CH_2 groups relatively to the ones of CH_3 at 0.9 ppm. This ratio is proportional to the relative number of protons, giving indications on the length of hydrocarbon chains present here. If one does not consider the small and broad peak present between 1.12 and 1.17 ppm, then one finds a ratio of 2.07 (inset of Figure 1a) that could be assigned to octane (C_8H_{18}) of size 0.655 nm in linear configuration. Moreover, one notes in this aliphatic range two doublets due to J couplings of 9 and 12 Hz for the CH_3 and CH_2 groups, respectively. These doublets are indicative of indirect spin−spin couplings of CH_3 or CH_2 protons with a close CH proton via bonding electrons. A possible example could be due to isooctane molecule. We compare in Figure 1b the ^{1}H NMR spectra of bulk crude oil with (sample 1) and without (sample 2) asphaltene and found a ratio ∼0.097 of intensities between the small peak around (1.12 to 1.17 ppm) and the sum of the other two well -resolved aliphatic peaks.

dx.doi.org/10.1021/jp311910t | J. Phys. Chem. B 2013, 117, 7002−7014

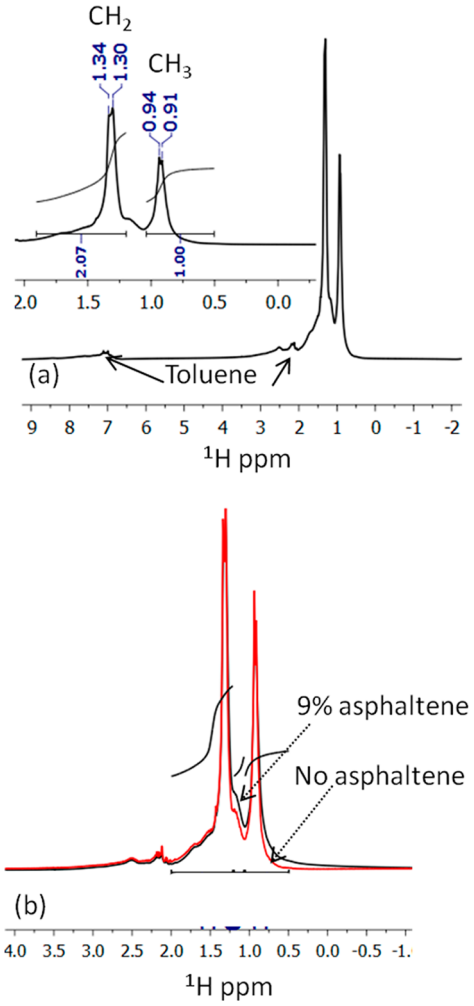

Figure 1. (a) ^{1}H NMR spectrum at 300 MHz of crude oil with 9% asphaltene. A small amount of deuterated toluene d_8 has been added to facilitate the assignments. CH_3 and CH_2 peaks are clearly assigned at 0.9 and 1.3 ppm, respectively. A ratio of 2.07 from the integration of CH_2 peaks is shown relatively to the CH_3 peaks at 0.9 ppm. A zoom of the aliphatic range is shown in the inset, where one clearly sees the J-coupling doublets of 12 and 9 Hz for the CH_2 and CH_3 peaks. (b) Comparison of the NMR spectrum at 300 MHz of crude oil with and without asphaltene.

Such a ratio almost corresponds to the amount of 9% of asphaltene found from chemical analysis. The main difference of the two spectra displayed in Figure 1b consists of the narrowing of the two main aliphatic peaks and the net decrease in the small peak around 1.17 ppm. Such a narrowing could be due to the quasi-absence of asphaltene macro- and nano-aggregates, thus enhancing the rotational dynamics of the hydrocarbons.

1D ^{13}C NMR Spectrum. ^{13}C NMR spectrum is divided into two main domains: aliphatic (5−60 ppm) and aromatic (100−160 ppm) carbons. Previous ^{13}C NMR spectra have been done for measuring the relative amount of nonprotonated and protonated carbon in the aromatic region of the spectrum where the asphaltene is supposed to stand.[26] Here we are interested only in evidencing a significative difference between the amount of all ^{13}C in crude oil with and without asphaltene. For that purpose, we perform on a Bruker Avance 600 NMR spectrometer the 1D ^{13}C NMR spectrum of crude oil with 9% asphaltene (sample 1) using a spectral width of 160 ppm (Figure 2a). Similarly, we show in Figure 2b the 1D ^{13}C NMR spectrum of crude oil without asphaltene (sample 2). One

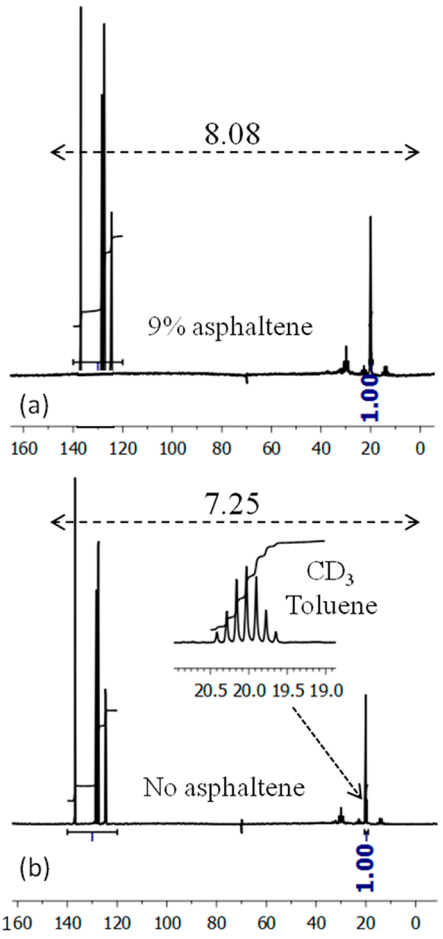

Figure 2. ^{13}C NMR spectrum of crude oil at 600 MHz with 9% asphaltene (a) and 0% asphaltene (b). In the inset, we show the septuplet, around 20 ppm, due to the coupling of the ^{13}C with the three methyl deuterons. In both Figures, the intensities of total carbons are indicated relatively to the ones of the septuplet.

notes in both cases a septuplet (inset of Figure 2b), around 20 ppm, corresponding to the coupling to the methyl group of the perdeuterated toluene. The comparison of intensities of all ^{13}C on both spectra relative to the intensity 1 of the septuplet shows an increase of 11.4% on sample 1 relative to sample 2. This percentage is in the same range as those (9%) found by a chemical analysis.

3. Standard Gas Chromatography and Gel Permeation Chromatography. The standard GC is very well suited to analyze low viscosity oils (here 25 cP) that contain only negligible quantity of large molecules. We show in Figure 3 GC data of sample 1 reporting the percentage of moles of hydrocarbons up to molecules with 30 carbons in either linear or isomeric configurations. The GPC data are also plotted in Figure 3 for extending the range of chain lengths up to C300. In that case, Figure 3 includes the contribution of asphaltenes. To clarify the Figure, we have omitted the data between C75 and C300, representing only 1.37%. The observed highly skewed distribution of carbon number or chain length is typical of a log-normal distribution. However, a pdf built as a bimodal log-normal distribution is needed to fit the data of Figure 3:

dx.doi.org/10.1021/jp311910t | J. Phys. Chem. B 2013, 117, 7002−7014

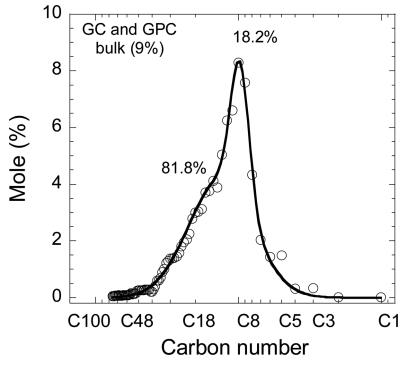

Figure 3. Standard gas chromatography (GC) of the bulk crude oil (9% asphaltene) reporting the percentage of moles of hydrocarbons up to molecules with 30 carbon atoms in either linear or isomeric forms. The gel permeation chromatography (GPC) data are also plotted for including the contribution of asphaltenes. The omitted data on the Figure between C75 and C300 represents only 1.37%. The continuous line is the best fit obtained with a superposition of two log-normal distributions (eq 1) whose parameters are described in Table 1.

$$f(x) = \sum_{i=1}^{2} \frac{C_i}{x\sigma_i\sqrt{2\pi}} \exp\left[-\frac{(\ln x - \mu_i)^2}{2\sigma_i^2}\right], \quad x > 0 \tag{1}$$

where C_i, μ_i, and σ_i are the dimensionless weighting concentration, the mean, and the standard deviation, respectively. The pdf $f(x)$ is normalized such as: $\int_{\min(x)}^{\max(x)} f(x)\,dx = C_1 + C_2$. The parameters extracted from the best fits of the data obtained with eq 1 are given in Table 1. We also give in Table 1 the ith mode defined as $e^{\mu_i - \sigma_i^2}$, which corresponds to the variable x (here the carbon number) of global maximum of each individual pdf. We find that the first one has a mode corresponding to (C_7, C_8) and represents 18.2% (in mole %) of the hydrocarbons. The second one has a mode corresponding to (C_{16}) and represents 81.8% (in mol %) of the hydrocarbons.

Table 1. Parameters Extracted from Equation 1 of the GC and GPC Data Shown in Figure 3a

parameters	GC and GPC data	mode i
C_1	18.2%	
σ_1	0.15	corresponds to C_8
μ_1	2.30	
C_2	81.8%	
σ_2	0.52	corresponds to C_{16}
μ_2	2.86	

4. 2D DOSY ^{1}H NMR. DOSY is a 2D NMR method that correlates the translational diffusion coefficient, D, with a resolved ^{1}H spectrum. The method is well-documented[21,22] and allows chemical resolution and identification of mobility of the different constituents in a mixture. The data shown in Figure 4a–c have been obtained on a Bruker Avance 300 MHz with a 5 mm DUL probe equipped with a Z gradient coil of 53.5 G/cm. We used the improved diffusion-ordered 2D sequence using stimulated echoes, longitudinal eddy current delay, and bipolar pulsed field gradients. The measurement involves the acquisition of a series of 64 FID echoes by varying the bipolar gradient strength in 64 steps from 2 to 95% of maximum intensity. Diffusion delay and recycle time between each acquisition are set to 20 ms and 5 s, respectively. The size of the data is 16k points in the acquisition dimension. For the processing software, we used the Topspin software of Bruker. Even though diffusion measurements are recorded as 2D data, they are basically a set of 1D spectrum with 16k*64 complex data. The processing starts by a classical Fourier transform in the acquisition domain, with zero filling of SI(F2) = 16k and

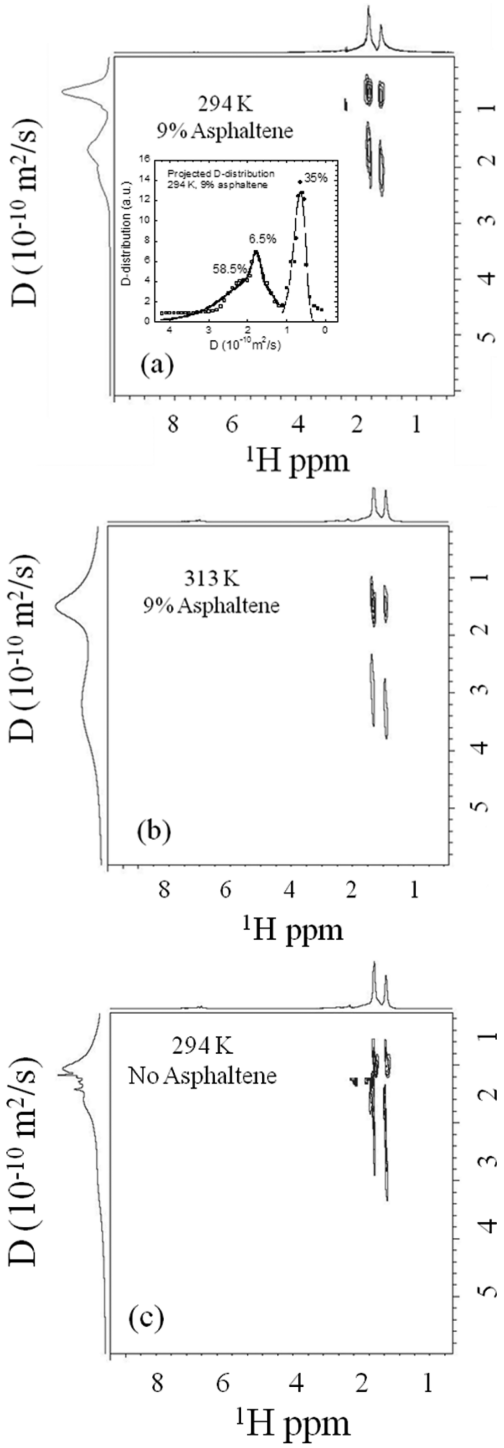

Figure 4. Two-dimensional DOSY NMR spectrum that correlates the ^{1}H NMR spectrum at 300 MHz and the distributions of translational diffusion coefficients obtained through a pulsed field gradient spin echo method with bipolar pulsed gradients. Results obtained on sample 1 at 294 (a) and 313 K (b) and at 294 K for sample 2 (c). We show in the inset of panel a the log-normal analysis of the projected D distribution whose parameters are described in Table 2.

dx.doi.org/10.1021/jp311910t | J. Phys. Chem. B 2013, 117, 7002–7014

SI(F1) = 1k and phase corrections in the F2 dimension. To obtain the DOSY spectrum, we fit all of the columns of the F2 transformed spectrum independently using a multiexponential Levenberg–Marquardt algorithm. The horizontal axis represents chemical shifts in ppm, and the vertical axis (linear scale) represents the diffusion coefficients in units of 10^{-10} m^2/s.

We show DOSY results on sample 1 at two temperatures in Figure 4a,b and the corresponding DOSY spectrum on sample 2 at room temperature in Figure 4c. We have displayed on the same scale and intensity the DOSY experiments with (Figure 4a,b) and without (Figure 4c) asphaltene. The projections of the ^1H spectrum and the distribution of the translational diffusion coefficients D are also shown in these Figures. We only observe DOSY peaks on the ^1H aliphatic range. No diffusion coefficients are measured for aromatic protons close to 7 ppm. In the case of asphaltene solutions, this latter observation was in favor of the continental model of asphaltenes, where aromatic cores are highly substituted.[9,10]

In the presence of asphaltene, this experiment allows us to identify two populations of hydrocarbons characterized by distributions of translational diffusion coefficients for CH_2 and CH_3 groups separated by a factor 2.64 and 3.0, respectively (Figure 4a). This shows that both groups, which are more or less constraints, belong to the same hydrocarbon aliphatic chain. Because of the large variety of hydrocarbons present in crude oil, one observes at 294 K two well-separated distributions of translational diffusion coefficients of intensities 35 and 65% centered on (0.65 and 1.9) × 10^{-10} m^2/s, respectively (Figure 4a). One observes a shift of the two distributions to higher values of D ((1.5 and 3.1) × 10^{-10} m^2/s) when increasing the temperature to 313 K. This is expected for an activated dynamical process. The structure of the spectrum at the higher temperature, even with broader distributions, is basically preserved, which rules out any local disentanglement of some local crystallization.

In the absence of asphaltene, the separation factor is reduced to 1.25 for CH_2 and 1.5 for CH_3 DOSY peaks. This distribution merging, as seen on the projection along the D axis (Figure 4c), thus evidences a single population. It seems that the slowest diffusion distribution almost disappears or at least merges to the fast one.

On the basis of the connection previously observed between diffusion and GC distributions in crude oils,[13] we will analyze the projected diffusion distributions of Figure 4a. We show in the inset of Figure 4a the best fits obtained with eq 1 either with a monomodal log-normal or a bimodal log-normal distribution of the two projected distributions of the translational diffusion coefficients D. The parameters extracted from this fit are given in Table 2. We also give in Table 2 the values of the modes corresponding to the variable D of global maximum of each individual pdf. For the low diffusion peak representing 35% of the hydrocarbons, we find a unique pdf with a mode at $D = 0.63 \times 10^{-10}$ m^2/s. For the higher diffusion peak, we find a bimodal pdf whose first mode stands at $D = 1.77 \times 10^{-10}$ m^2/s, representing 6.5% of the hydrocarbons. The second mode stands at $D = 1.85 \times 10^{-10}$ m^2/s, representing 58.5% of the hydrocarbons.

Table 2. Parameters Extracted from Equation 1 of the Projected DOSY Data Shown in Figure 4a

parameters	peak at low D	mode $e^{\mu_i-\sigma_i^2}$ at low D (10^{-10} m^2/s)	peak at high D	mode $e^{\mu_i-\sigma_i^2}$ at high D (10^{-10} m^2/s)
C_1	5.03 (35%)		0.74 (6.5%)	
σ_1	0.24	0.632	0.059	1.77
μ_1	−0.4		0.57	
C_2			6.76 (58.5%)	
σ_2			0.33	1.85
μ_2			0.72	

On a diffusion delay of Δ = 20 ms and with the diffusion coefficient found by these DOSY experiments, the translational diffusion is sufficiently fast for visiting all of the macroaggregates because the length of diffusion $l_D = (6D\Delta)^{1/2} \approx 5$ μm is much larger than the average distance, ∼50 nm, between two macroaggregates for an average concentration of 9% of asphaltene. The general shapes and the percentages of the modes of these projected diffusion distributions are in good agreement with the chain lengths distributions found from GC and GPC (Figure 3). So, all of the features displayed in Figure 4a could be consistent with two populations of hydrocarbons characterized by two distributions of diffusion coefficients. The slowest diffusion distribution could be due to a small proportion of small hydrocarbons interacting with the asphaltene nanoaggregates. The fastest diffusion distribution could be due to a larger proportion of hydrocarbons moving in between the asphaltene macroaggregates.

5. Nuclear Magnetic Relaxation Dispersion. Basically, proton NMR relaxation is a stimulated (nonspontaneous) phenomenon driven by the coupling of the proton spins to the magnetic noise induced by molecular motions (translation, rotation, exchange, etc.). Varying the magnetic field changes the proton angular Larmor frequency ω_I and thus allows us to explore the time scales of the magnetic fluctuations (noise) to which the longitudinal nuclear spin relaxation $1/T_1$ is sensitive. For diffusive liquids, NMRD also gives a rich source of dynamical information over a large range of length and time scales, from localized and fast motions at large frequency to delocalized and slow motions at low frequency. Furthermore, the magnetic-field dependence of the spin–lattice relaxation rate, $1/T_1$, provides a good test of the theories that relate the measurement to the microdynamical behavior of the fluid. This is potentially true in complex fluid such as crude oil, where the effect of reduced dimensionality may force more frequent reencounters of proton-spin bearing hydrocarbons either with paramagnetic species or with proton-surface groups on asphaltene nanoaggregates. These reencounters alter the correlation functions that directly govern the relaxation equation. Another important aspect here is the effect of the large distribution of chain lengths that will be at the origin of a large distribution of relaxation times.

We perform proton NMRD on a fast-field cycling spectrometer from Stelar s.r.l., Mede, Italy. All samples were introduced into sealed 10 mm-diameter standard NMR tubes. In the prepolarized mode (PP), the proton nuclear magnetization originally at thermal equilibrium is oriented toward the external steady polarized magnetic field (typically 0.5T) to achieve the initial value: M_z^{pol} (20 MHz). The external field is then instantaneously decreased (in ∼3 ms) to an evolution magnetic field chosen in the range from 0.25 mT to 0.5 T in which the longitudinal magnetization $M_z(\tau)$ relaxes to achieve the equilibrium value $M_z^{eq}(\omega_I)$ in the chosen angular frequency ω_I; then, the magnetic field is fixed to 0.25T in which a classical free induced longitudinal magnetization decay measurement is then achieved by applying a $\pi/2$ pulse. Such a fast field cycling sequence is very well-documented.[15] The temperature was fixed

dx.doi.org/10.1021/jp311910t | J. Phys. Chem. B 2013, 117, 7002–7014

at 298 K. The experiment was repeated over a large range of proton Larmor frequencies $\omega_I/2\pi$ (10 kHz to 15 MHz) to obtain the complete dispersion profile of the longitudinal spin−lattice relaxation rate $R_1(\omega_I) = 1/T_1(\omega_I)$. The non-pre-polarized mode (NP) is applied when the frequency is larger than 8 MHz. Here the longitudinal magnetization progressively reaches the equilibrium value. As multiple environments are sampled, the longitudinal magnetization evolves nonexponentially in either PP or NP modes according to the following integral equations:

$$M_z^{PP}(\omega_I, \tau) = M_z^{eq}(\omega_I) + [M_z^{pol}(15\ \text{MHz}) - M_z^{eq}(\omega_I)] \int f(T_1)e^{-\tau/T_1}\, dT_1 + \varepsilon(\tau), \quad \text{for } \nu_I < 8\ \text{MHz}$$

$$M_z^{NP}(\omega_I, \tau) = M_z^{eq}(\omega_I)[1 - \int f(T_1)e^{-\tau/T_1}\, dT_1] + \varepsilon(\tau), \quad \text{for } \nu_I \geq 8\ \text{MHz} \qquad (2a,b)$$

In eq 2a,b, $f(T_1)$ represents the distribution of spin−lattice relaxation times that will be found by using our own inversed Laplace transform method (ILT) and $\varepsilon(t)$ represents the random noise.

T_1 Distribution Obtained at Variable Larmor Frequencies. We show in Figure 5a−d some examples of the large distributions $f(T_1)$ found for bulk sample 1 at four different Larmor frequencies. Although the observed distribution reveals the distribution of hydrocarbons, we need two pdf's for fitting the data. The continuous lines in Figure 5a−d represent the best fits obtained with eq 1 with the extracted parameters given in Table 3. We also give in Table 3 the modes that correspond to the variable T_1 of global maximum of both individual pdf's. For instance, at 10 kHz, the first pdf has a mode $T_{1,\text{mode-1}}(10\ \text{kHz}) = 63.0$ ms representing 21.0% of the hydrocarbons, while the second pdf has a mode $T_{1,\text{mode-2}}(10\ \text{kHz}) = 33.8$ ms representing 79.0% of the hydrocarbons. These percentages are quite similar to the ones obtained from GC and GPC data (Figure 3). This proves that the hydrocarbon dynamics are correlated with the chain lengths. When increasing the Larmor frequency to 0.94 and 4.25 MHz, the modes of the first pdf increase progressively to 119.5 and 125.0 ms, with a proportion also increasing progressively to 43.4 and 89.9%, respectively. The modes of the second pdf decrease progressively to 49.4 and 17.7 ms, with a proportion decreasing also progressively to 56.6 and 10.1%, respectively. At 15 MHz, a fit is even achieved with a single log-normal distribution with a single mode at 113.0 ms. We have repeated the same procedure for 30 Larmor frequencies logarithmically equally spaced between 10 kHz and 15 MHz, and the results generalize the bimodal pdf distributions shown in Figure 5 that evolve significantly with the frequency. So, at low frequency the proportion of the second mode (C_2), at short T_1, dominates in comparison with the first mode (C_1) for large T_1. When the frequency increases, the situation changes progressively. The proportion of the first mode (C_1) increases, while the one of the second mode (C_2) decreases up to a point where a single mono-log-normal pdf can fit the data at large frequency. So there are two relaxation processes in the presence of asphaltene in sample 1.

To elucidate more precisely the origin of these two relaxation processes, we compare the effect of asphaltenes on the distributions $f(T_1)$ of sample 1 and sample 2 at 10 kHz (Figure 6a) and 15 MHz (Figure 6b). Similarly, we compare the effect of the confinement on the distributions $f(T_1)$ of sample 1 and sample 3 at 10 kHz (Figure 6c) and 15 MHz (Figure 6d). All of these Figures are plotted on similar axes to facilitate the comparisons. Basically, there are neither significant

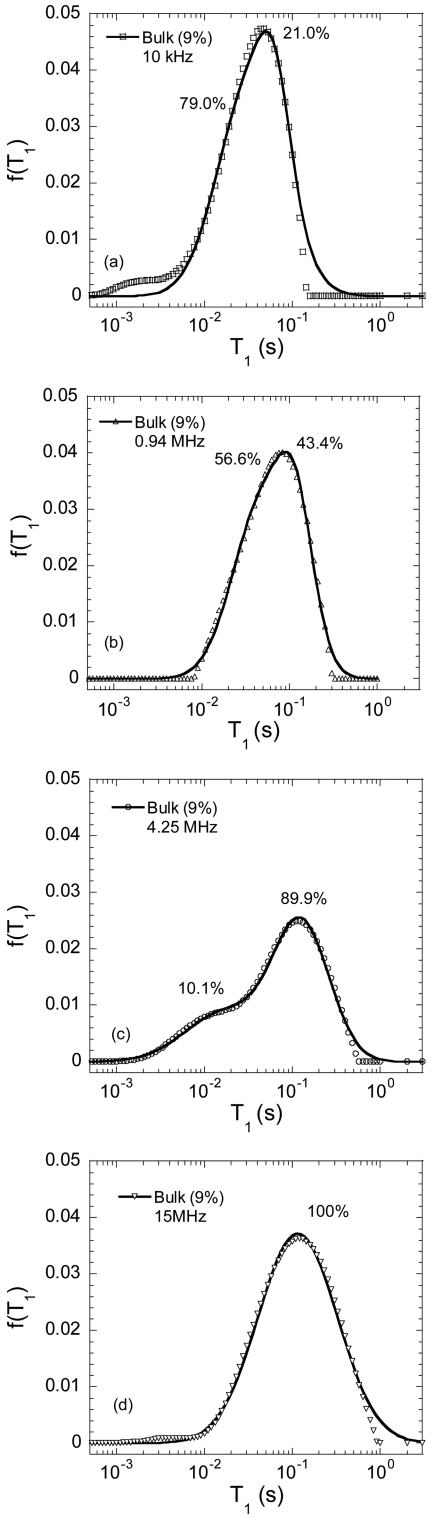

Figure 5. One-dimensional T_1 distributions obtained by ILT of the longitudinal magnetization decays of sample 1 measured at different frequencies labeled in the Figure. The continuous lines are the best fits obtained with a superposition of two log-normal distributions for 10 kHz (a), 0.94 MHz (b), and 4.25 MHz (c) and a single log-normal distribution for 15 MHz (d), respectively, whose parameters are described in Table 3.

dx.doi.org/10.1021/jp311910t | J. Phys. Chem. B 2013, 117, 7002−7014

Table 3. Parameters Extracted from Equation 1 of the Bulk 9% T_1 Data Shown in Figure 5

parameters	T_1 at 10 kHz	mode (ms) 10 kHz	T_1 at 0.94 MHz	mode (ms) 0.94 MHz	T_1 at 4.25 MHz	mode (ms) 4.25 MHz	T_1 at 15 MHz	mode (ms) 15 MHz
C_1	0.00105 (21.0%)		0.00314 (43.4%)		0.0071 (89.9%)		0.0185 (100%)	
σ_1	0.409	63.0	0.463	119.5	0.73	125.0	1.03	113.0
μ_1	−2.60		−1.91		−1.55		−1.12	
C_2	0.00395 (79.0%)		0.0041 (56.6%)		0.00076 (10.1%)			
σ_2	0.853	33.8	0.78	49.4	1.08	17.7		
μ_2	−2.66		−2.40		−2.87			

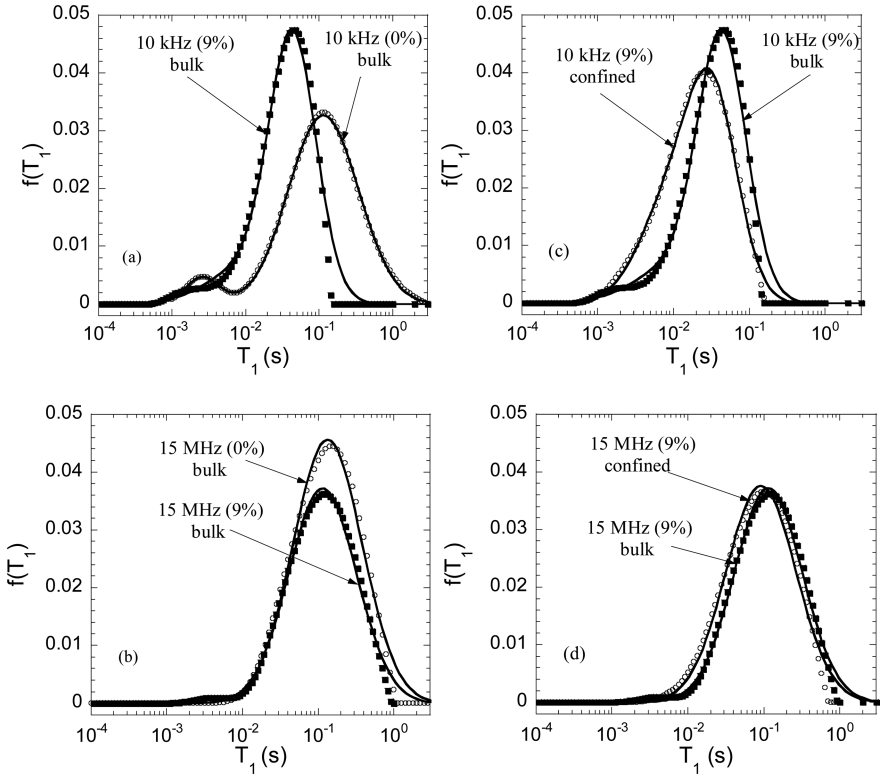

Figure 6. Comparisons of the 1D T_1 distributions obtained by ILT of the longitudinal magnetization decays of crude oil measured under different conditions (frequency, asphaltene percentage, bulk, and confinement in rocks). All data are reported on the same range of T_1 values to facilitate the comparison. (a) 10 kHz for 0 and 9% asphaltene. (b) 15 MHz for 0 and 9% asphaltene. (c) 10 kHz for 9% asphaltene in bulk and in confinement. (d) 15 MHz for 9% asphaltene in bulk and in confinement. The continuous lines are the best fits obtained with a superposition of either two or one log-normal distributions whose parameters are reported in Table4.

Table 4. Parameters from Equation 1 of the T_1 Data Shown in Figure 6a−d

parameters	T_1 at 10 kHz bulk 0%	mode (ms) 10 kHz bulk 0%	T_1 at 15 MHz bulk 0%	mode (ms) 15 MHz bulk 0%	T_1 at 10 kHz confined 9%	mode (ms) 10 kHz confined 9%	T_1 at 15 MHz confined 9%	mode (ms) 15 MHz confined 9%
C_1	0.023 (99.9%)		0.028 (100%)		0.025 (96.4%)		0.016 (100%)	
σ_1	1.09	116.0	1.05	132.0	0.74	35.0	1.06	90.4
μ_1	−0.97		−0.92		−2.81		−1.28	
C_2	$5.7 \times 10^{-5} \leq 0.1\%$				0.00094 (3.6%)			
σ_2	0.86	1.6			1.02	11.1		
μ_2	−5.69				−3.46			

asphaltene nor confinement effects at 15 MHz (Figure 6b,d). At 15 MHz, the distributions $f(T_1)$ of samples 1, 2, and 3 have been fitted with a single log-normal pdf centered around an average mode $T_1 \approx 112$ ms (Table 4). This confirms some previous results of Zielinski et al. on other crude oils without asphaltene.[20] The quantitative comparisons on the values of the proportions of the two modes in the T_1 distributions at low frequency (Figure 6a,c and Table 4) are now quite similar to the ones found from GC, GPC, and DOSY distributions as well as the previous ones found from GC and T_2 in other crude oils.[13]

All of the observations and fits described above and displayed in Figures 5 and 6 are compatible with a superposition of intramolecular and intermolecular contributions in the

dx.doi.org/10.1021/jp311910t | J. Phys. Chem. B 2013, 117, 7002−7014

longitudinal relaxation rates within this complex fluid. The intramolecular contribution that does not depend on frequency is representative of a fast reorientational relaxation process of individual hydrocarbons in bulk. The intermolecular contribution that depends on the Larmor frequency is mediated by the slow translational diffusion of the hydrocarbon protons in proximity of the paramagnetic species embedded within asphaltene nanoaggregates.

NMRD Profiles of <1/T1>. We show in Figure 7 the measured logarithmic average proton spin−lattice relaxation rate constants $<1/T_1\ (s^{-1})>$ as a function of the magnetic field plotted as the proton Larmor frequency for crude oil with samples 1−3 and sample 4 (reformed sample). We remind that the log-mean average $<1/T_1\ (s^{-1})>$ is defined as:

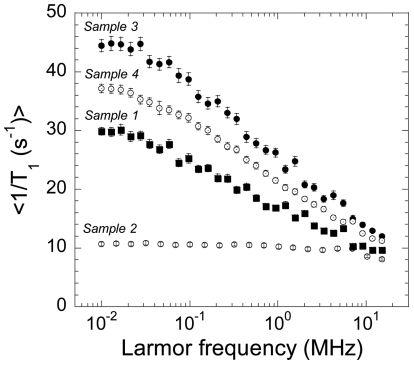

Figure 7. Measured logarithmic average proton spin−lattice relaxation rate constants $<1/T_1\ (s^{-1})>$ as a function of the magnetic field plotted as the proton Larmor frequency for crude oil for samples 1−4.

$$\langle 1/T_1(\omega_I)\rangle = \exp\left(-\sum_{i=1}^{n} f_i \ln T_{1,i}(\omega_I)\right) \quad (3)$$

where f_i is the ith value of the discretized $f(T_1)$ distribution at angular frequency ω_I. Of course there are other possibilities to define an average on these highly skewed $f(T_1)$ distributions. For instance, the median or the mode described above. Because of the extracted parameters values given in Table 3 and the noise level of the experiments there are no large differences between all of these different averages. The observed NMRD profiles shown in Figure 7 exhibit very different behaviors: from highly dispersed behaviors for samples 1, 3, and 4 (with asphaltene) to almost no frequency dependence for sample 2 (without asphaltene). One also notes a plateau for these NMRD profiles below 25 kHz. We repeat a large number of times the experiments to check the reality of these plateau. These striking different behaviors have been recently observed for other crude oils,[20] but a complete interpretation has not been proposed so far. One of the main issues of this study is thus to propose an interpretation of these NMRD profiles on the basis of an original theoretical model described below.

III. THEORY AND DISCUSSION OF NMRD DATA IN BULK AND CONFINED CRUDE OILS IN PRESENCE OF ASPHALTENE

We first aim at interpreting theoretically the NMRD experiments of the log-mean average $<1/T_1(\omega_I)>$ of Figure 7 for bulk crude oil with asphaltene (sample 1). For each frequency, the log-mean values of $<1/T_1(\omega_I)>$ stay very close to the ones obtained for the mode of the dominant log-normal distribution. We saw in Figure 3 that the dominant carbon number for the hydrocarbons corresponds to octane C_8. This means a chain length $\delta_{oil} \approx 0.655$ nm. Although we have observed highly skewed distributions $f(T_1)$ (Figures 5 and 6), the NMRD profiles $<1/T_1(\omega_I)>$ follow the frequency dependence of a $T_1(\omega_I)$ value close to the maximum of the distribution $f(T_1(\omega_I))$, which means that we can restrict our theoretical approach to a given hydrocarbon of average size δ_{oil} for the interpretation of the data of Figure 7.

1. Model. For samples 1, 3, and 4, the quasi-logarithmic behavior of the ^{1}H NMRD data at low frequency (Figure 7) strongly suggests the hypothesis of a reduced dimensionality,[16] maintaining at long time (low frequency) the pairwise dipolar correlation between the moving proton-spin bearing hydrocarbons and some immobile paramagnetic species uniformly distributed within aromatic parts of oblate asphaltene nanoaggregates. Usually, in crude oils, these paramagnetic species are embedded in metal-porphyrine (MP) compounds or correspond to stable radicals. Recent combined liquid chromatography profiles coupled to a mass spectrometer with an ICP detector technique were used for evidencing the trapping of MP by asphaltene aggregates.[27] In particular, extensive overlapping with sulfur profiles was observed for a part of vanadium and all nickel profiles on significant time scales, thus suggesting that these MP compounds are interlocked with the polar parts of asphaltene aggregates in solution.[27] Even if the concentration of vanadium could be very low, the localization of this paramagnetic species trapped in MP within the abundant asphaltene nanoaggregates (here 9 wt %) could drastically enhance their local concentration at the origin of the heteronuclear nuclear magnetic relaxation NMRD profile.

In the presence of asphaltene, the dispersion of the NMRD at low field also requires a very slow rotational motion of the macroaggregates constituted by several oblate nanoaggregates. Otherwise, the rotation averages out all of the heteronuclear dipole−dipole interactions, and the dispersion disappears. In fact, the radius of ∼7.2 nm found by recent SAXS and SANS studies for such macroaggegates on asphaltene−toluene mixtures[4] fulfills such a slow rotational assumption. However, the size of the macroaggregates can vary depending on the type of oil and asphaltenes and method used to measure them. For instance, the radius of such macroaggregates was found to be 2.6 nm for oils in reservoirs.[6] One can estimate the rotational correlation time τ_{rot} for such a macroaggregate of hydrodynamic radius r_H with the Stokes−Einstein relation: $\tau_{rot} = 4\pi r_H^3 \eta/(3k_B T)$. This gives at 25 °C: τ_{rot} = 11.1 and 0.60 μs for r_H = 7.2 and 2.6 nm, respectively. Moreover, because of the fractal shape of the asphaltene macroaggregtes,[4,5,28] the value of τ_{rot} could even increase, which facilitates our hypothesis. We will see in Section III.3 that the 2D translational correlation time τ_m in the proximity of the asphaltene nanoaggregates will be on the order of $\tau_m \approx 8$ ns, which is much shorter than τ_{rot}, thus justifying our hypothesis.

The schematic diagram of Figure 8 could describe the transient local geometry and anisotropic dynamics that are sufficient to account for the quasi-2D features implied by the observed bilogarithmic magnetic field dependence of $<1/T_1(\omega_I)>$. Moreover, with the high asphaltene concentration 9% (wt) of sample 1, clusters of several asphaltene nanoaggregates exist (Figure 8), thus creating some voids or cavities, allowing a drastic enhancement of the local concentrations of MP and paramagnetic species as well. This enhances in consequence the

dx.doi.org/10.1021/jp311910t | J. Phys. Chem. B 2013, 117, 7002−7014

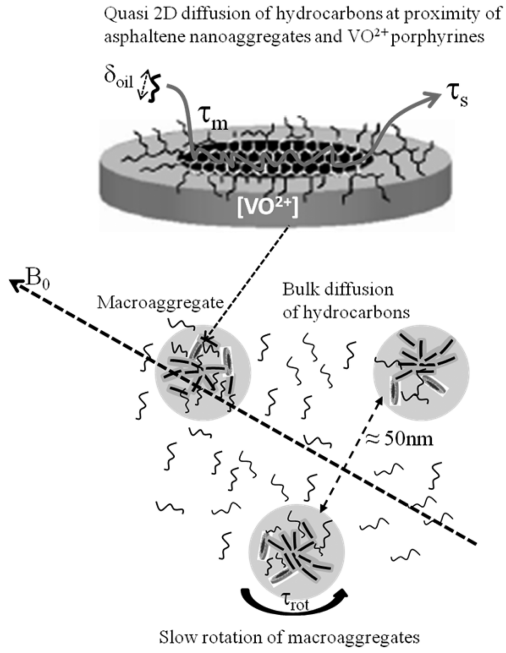

Figure 8. Schematic diagram describing the relaxation model used to fit the NMRD profile of crude oil with asphaltene. The shapes and sizes of asphaltene nanoaggregates and macroaggregates are inspired from ref 4. The dashed lines displayed on top describe the 2D translational diffusion of hydrocarbons at the surface of asphaltene nanoaggregates. The curved arrow (bottom) describes the slow rotational dynamics of asphaltene macroaggregates. The two populations of hydrocarbons transiently moving in the proximity of the surface of oblate nanoaggregates in the macroaggregates and in the bulk are also reported in the Figure.

probability of reencounters between proton hydrocarbons and paramagnetic species, not necessarily in first neighbor, for maintaining the pairwise dipolar correlations for a much longer time and thus causing the dispersion of NMRD at low frequency. The fractal character of these macroaggregates, evidenced by conductivity[28] and SAXS[4] measurements, favors the presence of such cavities. The plateau observed in the 2D NMR $D-T_2$ spin correlation spectra of samples 1 and 3, for long T_2, gives another evidence that hydrocarbons with small chains can transiently wet the asphaltene nanoaggregates.[29]

Consider proton spins $I = 1/2$ belonging to hydrocarbon chain of average size, δ_{oil}, in a given crude oil fluid of uniform density ρ_{oil} that diffuse in the proximity of the asphaltene nanoaggregates and macroaggregates in the presence of a constant magnetic field, $\boldsymbol{B}_0$ (Figure 8). We also consider the presence of a very small quantity of fixed paramagnetic species of spins, S, uniformly distributed within the polar parts of these nanoaggregates with a surface density σ_s. On the basis of all of the previous results described above, we consider two hydrocarbon populations. The first and dominant population is represented by the bulk hydrocarbons that stay in between the macroaggregates (Figure 8). Recent SAXS and SANS studies have shown that these macroaggregates stick up to 10 to 12 asphaltene molecules in a fractal network.[4] The second and small population is represented by the hydrocarbons transiently present within the asphaltene macroaggregates. The anisotropical translational dynamics of these hydrocarbons is highly influenced by the presence of these nanoaggregates. For sure, in the absence of asphaltene (sample 2), only the first population remains. Because the magnetic moment of the paramagnetic species is large ($\gamma_S = 658.21\gamma_I$), there is no ambiguity about the relaxation mechanism for the diffusing proton spins, I, which is the intermolecular dipolar relaxation process induced by fixed spins, S, and modulated by the translational diffusion of the mobile spins, I, in close proximity to these surfaces.

2. Relaxation Equations. In the following, we present a self-contained outline of the basic hypothesis and equations of the model needed for interpreting the NMRD data. Apart from the specificities of the crude oils studied, most of the details of the relaxation equations can be found elsewhere.[16]

(i) Basically, when considering the nuclear relaxation of a proton-liquid diffusing in the proximity of a solid surface, there are coupled relaxation equations for the solid and liquid magnetizations. The return to equilibrium of either solid or liquid proton spin magnetization is thus a bilinear combination of exponentials with the rate constants for slow ($R_{1,slow}$) and fast ($R_{1,fast}$) components given by:[30]

$$R_{1,\mathrm{slow/fast}} = \frac{1}{2}\{1/T_{1,s} + 1/T_{1,oil} + k(1 + 1/F) \mp [[1/T_{1,s} - 1/T_{1,oil} - k(1 - 1/F)]^2 + 4k^2/F]^{1/2}\} \quad (4)$$

Here $1/T_{1,s}$ and $1/T_{1,oil}(\omega_I)$ are the spin−lattice relaxation rate constants associated with solid protons attached to the asphaltene nanoaggregates and oil-protons, respectively. k is the dipolar cross-relaxation rate from the oil protons to the solid proton species in the vicinity of the surface of asphaltene nanoaggregates, and F is the ratio of the solid-proton magnetization to the liquid-proton magnetization at equilibrium: $F = m_s^{eq}/m_w^{eq} \ll 1$.

(ii) In most applications of field cycling experiments, the rapidly decaying component R_{fast} of the biexponential decay is not detected because of instrumental limitations, and the slowly decaying component R_{slow} dominates the observations. Moreover, for the surface liquid, the intermolecular dipole−dipole interaction couples the oil spin relaxation to that of the solid (asphaltene) and the magnetic field dependence of the immobilized solid spin system. From a theoretical point of view, the system reaches a long correlation time limit typical of the rigid-lattice limit $1/\omega_d \approx 6.4\ \mu s$ when the Larmor frequency is lower than the dipolar frequency $\omega_d/2\pi \approx 25$ kHz and for $k \ll 1/T_{1,s}$, $1/T_{1,oil}$, $|1/T_{1,oil} - 1/T_{1,s}|$, and $F \ll 1$. The cross-relaxation becomes very efficient ($k/F \gg k$) and is only limited by the transfer of dipolar energy (spin diffusion): R_{slow} ($\omega_I < \omega_d$) $\approx 1/T_{1,s} + k/F$, where one has by continuity $1/T_{1,s} \approx 1/T_{1,oil}$ ($\omega_I = \omega_d$). The observed plateau below ω_d is thus characteristic of the quasi-rigid lattice limit of the solid proton in the nanoaggregates. The absolute value of such a plateau is thus indicative of the specific surface area at the solid−liquid interface. The molecular exchange between the surface and bulk liquid phases is sufficiently fast compared with their respective individual proton relaxation times that a single $1/T_{1,oil}(\omega_I)$ exists given by a linear combination of a bulk and a surface contributions:[16]

$$\frac{1}{T_{1,oil}(\omega_I)} = \frac{1}{T_{1,bulk}} + \frac{N_S}{N}\frac{1}{T_{1,surf}(\omega_I)} \quad (5)$$

In eq 5, N_S/N represents the ratio of the number N_S of oil molecules transiently present in the proximity of the solid surface of asphaltene nanoaggregates over the total number, N, of exchangeable oil molecules in the sample. One can express such a ratio as $N_S/N = \delta_{oil}\,\rho_{oil}\,S_{p,NMR}$, where $S_{p,NMR} = S_pF$ is an NMR-based specific surface area[31] of the asphaltene nano-

dx.doi.org/10.1021/jp311910t | J. Phys. Chem. B 2013, 117, 7002−7014

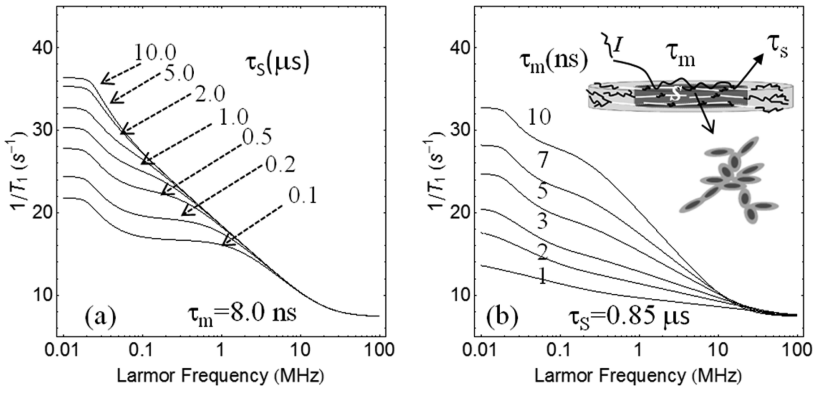

Figure 9. (a) Typical examples of theoretical NMRD calculated with eqs 4 and 6 using typical values corresponding to sample 1: δ_{oil} = 0.655 nm, $R_{1,bulk}$ = 7.2 s^{-1}, $S_{p,NMR}$ = 8.6 m^2/g, τ_m = 8 ns, and increasing values of the surface correlation time of residence τ_s from 0.1 to 10 μs. (b) Theoretical NMRD data calculated with eqs 4 and 6 when τ_s = 0.85 μs and increasing values of the 2D translational surface correlation time τ_m from 1 to 10 ns. The inset shows a schematic diagram, inspired by ref 4, of the quasi-2D diffusion relaxation model of hydrocarbon protons (I) in the proximity of the paramagnetic (S) species embedded within the aromatic part of the asphaltene nanoaggregate. The macroaggregate is also schematically represented as an ensemble of several nanoaggregates.

aggregates that appears to be directly proportional to $F \ll 1$ and the real specific surface area S_p of the asphaltene nanoaggregates.

(iii) The spin−lattice relaxation rate $1/T_{1,oil}(\omega_I)$ for the confined proton-liquid has a bilogarithmic frequency dependence[16,31] that comes unambiguously from the 2D diffusion of the oil molecules in the proximity of asphaltene nanoaggregate surface modulating the dipole−dipole interaction between the proton species and the paramagnetic species fixed within the polar part of the asphaltene nanoaggregates. The presence of heteroatoms like sulfur and nitrogen with lone pairs of electrons can induce van der Waals interactions that can polarize the hydrocarbon chains in the proximity of the polar and aromatic part of the asphaltene nanoaggregates. This weak and dispersive interaction can create a surface layer of hydrocarbons in the proximity of the oblate asphaltene nanoaggregates that could explain the lateral diffusion of hydrocarbons. This layer also favors the stabilization of crude oil asphaltenes in apolar alkanes solvents.[32,33] On the contrary, in the frequency range studied, the spin−lattice relaxation rate for the solid protons $1/T_{1,s}$ does not depend on the frequency,[31] and the bulk relaxation rate $1/T_{1,bulk}$ is frequency-independent.[34]

Taking all of these considerations into account, we find that the following theoretical analytical expression of $1/T_{1,oil}$ when substituted in eq 5 allows us to reproduce all of the observed frequency features:

$$1/T_{1,oil}(\omega_I > \omega_d) = 1/T_{1,bulk} + \frac{\pi}{30\delta_{oil}^3}\sigma_s\rho_{oil}S_{p,NMR}(\gamma_I\gamma_S\hbar)^2 S(S+1) \times \tau_m\left[3\ln\left(\frac{1+\omega_I^2\tau_m^2}{(\tau_m/\tau_s)^2+\omega_I^2\tau_m^2}\right) + 7\ln\left(\frac{1+\omega_s^2\tau_m^2}{(\tau_m/\tau_s)^2+\omega_s^2\tau_m^2}\right)\right] \quad (6)$$

Here σ_s is the surface density of paramagnetic impurities within the nanoaggregates. ρ_{oil} is the density of the crude oil, and δ_{oil} is the average hydrocarbon molecular size at the peak of the distribution. The electronic spin, S, depends on the nature of the paramagnetic species and can be identified by electronic spin resonance (ESR) spectrum. Because the gyromagnetic ratio of the electron, γ_S, is much larger than that of the proton, γ_I ($\gamma_S = 658.21\gamma_I$), the electronic Larmor frequency is also much larger than the nuclear one $\omega_S = 658.21\omega_I$. Also, in eq 6, τ_m is the correlation time characterizing the 2D diffusion of the proton species in the proximity of surfaces of the asphaltene nanoaggregates. We also introduce the effects of the finite time of residence $\tau_s \gg \tau_m$ for the mobile proton species in the proximity of surfaces of nanoaggregates by an exponential cutoff in the time dependence of the pair correlations between the mobile proton and the immobile paramagnetic species. The relaxation rate in the bulk phase, $1/T_{1,bulk}$, is caused by the superposition of fast molecular reorientations and translations and is independent of frequency in the low-field range studied.[34] Last, substituting eq 6 into eq 5 gives the theoretical expression that we can compare with the experiments in Figure 7.

We have displayed in Figure 9a the theoretical NMRD profiles, $1/T_1(\omega_I) = R_{1,slow}(\omega_I)$, calculated with eqs 4 and 6 using typical values corresponding to crude oil with 9% asphaltene: δ_{oil} = 0.655 nm, $R_{1,bulk}$ = 7.2 s^{-1}, $S_{p,NMR}$ = 8.6 m^2/g, F = 0.1, k = 0.1, τ_m = 8 ns, and increasing values of the surface correlation time of residence τ_S from 0.1 to 10 μs. We show in Figure 9b the corresponding theoretical NMRD profiles, $1/T_1(\omega_I) = R_{1,slow}(\omega_I)$, calculated with eqs 4 and 6 using the same parameters as in Figure 9a but with fixed values of τ_s = 0.85 μs and increasing values of the 2D translational surface correlation time τ_m from 1 to 10 ns. These theoretical NMRD profiles (Figure 9) thus evidence very different effects of these two correlation times that allow an easy determination from the experimental data.

3. Results and Comparison with Theory. The comparison of the magnetic field dependencies of the log-average proton spin−lattice relaxation rates $<1/T_1(\omega_I)>$ for samples 1−4 with the relaxation eqs 4 and 6 is reported in Figure 10.

For sample 1 (with 9% asphaltene), we used the following parameters. The oil density is measured as ρ_{oil} = 0.85 g/cm^3 at 25 °C. The average size of hydrocarbon chain corresponding to the main peak of the distribution $f(T_1)$ is chosen as δ_{oil} = 0.655 nm. We measured $1/T_{1,bulk}$ = 7.2 s^{-1} at large frequency. In eq 6, $S_{p,NMR} = S_pF \approx 8.6$ m^2/g is an NMR-based specific surface area of the asphaltene nanoaggregates that appears to be directly

dx.doi.org/10.1021/jp311910t | J. Phys. Chem. B 2013, 117, 7002−7014

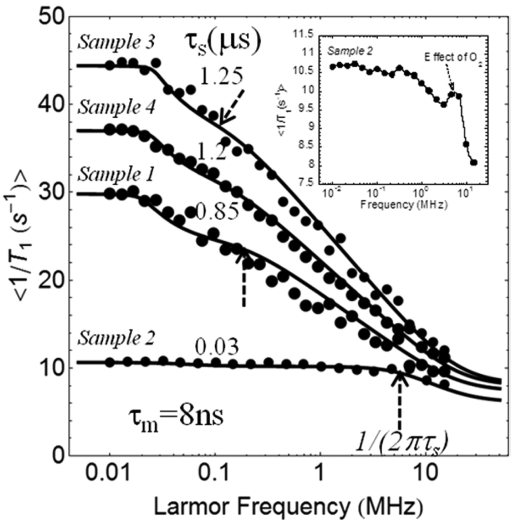

Figure 10. Measured logarithmic average proton spin−lattice relaxation rate constants $<1/T_1(s^{-1})>$ as a function of the magnetic field plotted as the proton Larmor frequency for samples 1−4. The continuous lines are the best fits obtained with eqs 4 and 6 and the model described in the text. The three arrows represent the respective values of $1/(2\pi\tau_s)$. The inset shows a zoom of the NMRD data of sample 2 evidencing the small peak around 10 MHz due to the presence of paramagnetic oxygen or trapped ions.

proportional to $F = 0.1$. Considering the nature and quantity of paramagnetic species, previous ESR spectra have evidenced different paramagnetic species such as VO^{2+} and stable free radicals in crude oils with asphaltene.[35] The nature of the paramagnetic VO^{2+} species can be potentially identified by the hyperfine interaction between the electron spin $S = 1/2$ delocalized in the aromatic π orbital and the nucleus of V^{51} ($I = 7/2$). Organic free radicals are also present in the fraction of oils, but their nature is not very well-known due to the multiplicity of molecular structures that causes the unresolved ESR single line.[36] We restrict our calculation to the case of highly diluted paramagnetic species where the average distance between two S spins on the surface, $1/\sqrt{\sigma_s} \approx 2.55$ nm, stays on the order of the average radius of the nanoaggregates. This assumption gives a paramagnetic species density conform to the quantitative measurements.[37] In eq 4, the dipolar cross-relaxation rate, $k \approx 0.1$, is chosen such that the cross-relaxation becomes very efficient ($k/F \gg k$) when the angular Larmor frequency becomes smaller than the dipolar frequency $\omega_d/2\pi \approx 25$ kHz. This could explain the crossover to the plateau observed at low frequency in Figure 10. Finally, we varied the correlation times and found $\tau_m = 8$ ns and $\tau_s = 0.85$ μs characterizing the 2D diffusion of the proton species in the proximity of the surface of the asphaltene nanoaggregates and the finite time of residence $\tau_s \gg \tau_m$, respectively. We note by a dashed arrow in Figure 10 the frequency, $1/(2\pi\tau_s) = 0.19$ MHz, that is inversely proportional to the time of residence of hydrocarbons on the asphaltene surfaces. The position of such a frequency corresponds exactly to the frequency of transition between the profiles coming from the electronic (ω_S) and nuclear (ω_I) parts of the spectral densities of eq 6.

One can define an average distance $r_{2D} \approx [4D_{surf}\tau_s]^{1/2}$ explored by the diffusion of hydrocarbons in the proximity of the surface of the oblate asphaltene nanoaggregates on a time τ_s ($\gg \tau_m$), where D_{surf} is the translational diffusion coefficient of hydrocarbons in the proximity of the asphaltene surfaces. At the molecular level, we have a similar relation, $\delta_{oil} \approx [4D_{mol}\tau_m]^{1/2}$, where D_{mol} is the molecular translational diffusion coefficient given by the Stokes−Einstein relation. From these two relations, one has: $r_{2D}/\delta_{oil} \approx [D_{surf}\tau_s/(D_{mol}\tau_m)]^{1/2}$. From the above NMRD analysis of sample 1 one finds $\tau_s/\tau_m \approx 106$, so $r_{2D}/\delta_{oil} \approx 10.3[D_{surf}/D_{mol}]^{1/2}$. Now, we have evidenced from the DOSY experiment in the presence of asphaltene and on a different time and length scales two populations of hydrocarbons characterized by diffusion coefficients that differ by a factor of three. The first population interacts with the asphaltene interface, and the second is free to diffuse in between the macroaggregates. Provided that the dynamics is scale invariant, one can thus conserve the relation $D_{surf}/D_{mol} \approx 1/3$ on the NMRD time and length scales. This reduces the distance explored by the diffusion of hydrocarbons to $r_{2D} \approx 3.9$ nm. Although NMR relaxation is not spatially resolved, the extraction of a time cutoff (τ_s) in the observed NMRD profiles, for which the dipolar correlation between I and S spins disappears, introduces a length scale r_{2D} that makes sense. Moreover, this distance is on the same order as the one, 3.2 nm, found from SAXS and SANS measurements of average size of asphaltene nanoaggregates in asphaltene solutions.[4] This value of r_{2D} is also not very far from the one ∼2.6 nm recently obtained, at higher temperatures for the asphaltene cluster sizes by observing the gravitational gradients of asphaltenes in oilfield reservoirs.[6]

For sample 2 (with 0% asphaltene), the situation is much more simple. The asphaltene macroaggregates disappear, and even the nanoaggregates become very rare. Moreover, we show in Section II.5 and Tables 3 and 4 that one can fit the distribution $f(T_1)$ by a single log-normal distribution that is independent of the Larmor frequency. The NMRD profile shown in Figure 10 has almost no frequency dependence with exception of the typical high-frequency tail and the typical bump (see the inset of Figure 10) induced by the nuclear paramagnetic relaxation due to dissolved paramagnetic oxygen or trapped ions.[38,39] This typical NMRD effect thus confirms the shortening of the relaxation times observed in light crude oils with long relaxation times.[40] This general behavior is typical of a fast hydrocarbon reorientational intramolecular relaxation process for all of the hydrocarbons. The continuous line displayed for sample 2 in Figure 10 has been obtained with a different $1/T_{1,bulk} = 6$ s^{-1} due to the decrease in viscosity, with the same $\tau_m = 8$ ns as sample 1 but with a very short $\tau_s = 30$ ns that reflects the quasi absence of the 2D diffusion. The dashed arrow in Figure 10 is thus shifted to a much higher frequency $1/(2\pi\tau_s) = 5.3$ MHz. In the limit where τ_S is on the same order as, although larger than, τ_m, the frequency dependence of eq 6 almost disappears and our theoretical 2D model tends to the usual 3D ones.

For sample 3 (confined crude oil with 9% asphaltene), the NMRD profile looks similar to the one of sample 1 (Figure 10), except for the enhancement of the absolute value of the profile. We succeed to renormalize the data of sample 1 to the one of sample 3 by an enhancement of just 63% of the specific surface area and an increase of $\tau_s = 1.25$ μs. The dashed arrow in Figure 10 is thus shifted to a lower frequency $1/(2\pi\tau s) = 0.13$ MHz, corresponding to the time of residence of hydrocarbons on both the asphaltene and pore surfaces. We explain the significative enhancement of τ_s by the presence of Fe^{3+} paramagnetic species on the rock-pore surface.

For sample 4 (reformed bulk sample), the NMRD profile shown in Figure 10 looks similar to the one of sample 1. The

dx.doi.org/10.1021/jp311910t | J. Phys. Chem. B 2013, 117, 7002−7014

small difference with results of sample 1 is due to some small losses in the recombination process. The signal-to-noise is even increased due to the homogenization of the chemical preparation. This allows us to evidence much more clearly the presence of a plateau at low field that is predicted by the theory (eqs 4 and 6).

IV. CONCLUSIONS

Multiscale NMR techniques have proven to be useful for estimating the complex structure and multidynamics of proton species in bulk and confined crude oils with and without asphaltene. High-field 1D and 2D NMR spectroscopies have characterized the proton and carbon species of crude oils with and without asphaltene. 2D DOSY spectra have allowed us to identify two populations of hydrocarbons, characterized by two distributions of translational diffusion coefficients in the presence of asphaltene and a single one without asphaltene. A detailed analysis of the distributions of longitudinal relaxation time, T_1, measured at variable magnetic fields by the NMRD technique is proposed in terms of a bimodal log-normal distribution whose parameters confirm the two environments evidenced by DOSY spectra. The remarkable features of the NMRD profiles of $1/T_1$ for bulk and confined crude oils with and without asphaltene have been interpreted in terms of an original model of different processes of intermittent surface dynamics of proton species in the proximity of the surface of asphaltene nanoaggregates and bulk dynamics in between the clusters of these nanoaggregates. The comparison of our NMRD data with such a theoretical model has allowed us to find the 2D translational diffusion correlation time as well as the time of residence of the hydrocarbons in the proximity of the surface of asphaltene nanoaggregates. Provided that the diffusion of the hydrocarbons close to the asphaltene nanoaggregates is three times smaller than the bulk diffusion, as the DOSY experiments show, this latter time gives an average radius of exploration for the 2D hydrocarbon diffusion, $r_{2D} \approx 3.9$ nm, on the same order of magnitude as the sizes found by J. Eyssautier with SAXS and SANS in asphaltene solutions and by O. C. Mullins at higher temperatures by the observation of gravitational gradients of asphaltenes in oilfield reservoirs.

AUTHOR INFORMATION

Corresponding Author

*E-mail: jean-pierre.korb@polytechnique.fr. Tel: 33 1 69 33 47 39.

Notes

The authors declare no competing financial interest.

ACKNOWLEDGMENTS

We acknowledge D. Grebenkov (CNRS, Palaiseau) for his help in the inverse Laplace transform algorithm. Many thanks for H. Zhou (Total, EP) and B. Bouyssiere (CNRS, Pau) for stimulating discussions about the trapping of metallic porphyrins by asphaltene aggregates. We thank J. Eyssautier and P. Levitz for private communications about their SAXS and SANS data. Special thanks to M. Hürlimann (SDR Schlumberger), A. Kurup, A. Valori, and N. Bachman (SDCR, Schlumberger) for stimulating discussions on crude oils. The crude oils were provided by Total (France).

REFERENCES

(1) Grob, R. L.; Barry, E. F. *Modern Practice of Gas Chromatography*, 4th ed.; Wiley-Interscience: Hoboken, NJ, 2004.
(2) Marshall, A. G. Milestones in Fourier Transformation Cyclotron Resonance Mass Spectroscopy Technique Development. *Int. J. Mass Spectrom.* **2000**, *200*, 331−356.
(3) *Asphaltene, Heavy Oils and Petroleomics*; Mullins, O. C., Sheu, E. Y., Hammami, A., Marshall, A. G., Eds.; Springer: New York, 2007.
(4) Eyssautier, J.; Levitz, P.; Espinat, D.; Jestin, J.; Gummel, J.; Grillo, I.; Barré, L. Insight into Asphaltene Nanoaggregate Structure Inferred by Small Angle Neutron and X-Ray Scattering. *J. Phys. Chem. B* **2011**, *115*, 6827−6837.
(5) Eyssautier, J. Caractérisation et Modélisation des Asphaltènes en Conditions Réactionnelles d'Hydrotraitement. Ph.D. Thesis, Ecole Polytechnique, Palaiseau, January 2012.
(6) Mullins, O. C.; Seifert, D. J.; Zuo, J. Y.; Zeybeck, M. Clusters of Asphaltene Nanoaggregates Observed in Oilfield Reservoirs. *Energy Fuels* **2012**, *27*, 1752−1761.
(7) Silva, R. C.; Seidl, P. R.; Menezes, S. M. C.; Teixeira, M. A. G. ^{1}H and ^{13}C NMR for Determining Average Molecular Parameters of Asphaltene from Vacuum Residue Distillation. *Ann. Magn. Reson.* **2004**, *3*, 63−67.
(8) Lisitza, N. V.; Freed, D. E.; Sen, P. N.; Song, Y. Q. Study of Asphaltene Nanoaggregation by Nuclear Magnetic Resonance (NMR). *Energy Fuels* **2009**, *23*, 1189−1193.
(9) Durand, E.; Clemancey, M.; Lancelin, J. M.; Verstraete, J.; Espinat, D.; Quoineaud, A.-A. Aggregation States of Asphaltenes: Evidence of Two Chemical Behaviors by ^{1}H Diffusion-Ordered Spectroscopy Nuclear Magnetic Resonance. *J. Phys. Chem. C* **2009**, *113*, 16266−16276.
(10) Durand, E.; Clemancey, M.; Lancelin, J. M.; Verstraete, J.; Espinat, D.; Quoineaud, A.-A. Effect of Chemical Composition on Asphaltene Aggregation. *Energy Fuels* **2010**, *24*, 1051−1062.
(11) Hürlimann, M. D.; Venkataramanan, L. Quantitative Measurement of Two-Dimensional Distribution Functions of Diffusion and Relaxation in Grossly Inhomogeneous Fields. *J. Magn. Reson.* **2002**, *157*, 31−42.
(12) Mutina, A. R.; Hürlimann, M. D. Correlation of Transverse and Rotational Diffusion Coefficient: a Probe of Chemical Composition in Hydrocarbon Oils. *J. Phys. Chem. A* **2008**, *112*, 3291−3301.
(13) Freed, D.; Hürlimann, M. D. One and Two-Dimensional Spin-Correlation of Complex Fluids and the Relation to Fluid Composition. *C. R. Phys.* **2010**, *11*, 181−191.
(14) Dunn, K. J.; Bergman, D. J.; Latorraca, G. A. Nuclear Magnetic Resonance Petrophysical and Logging Applications. In *Handbook of Geophysical Exploration*; Helbig, K., Tritel, S., Eds.; Pergamon: Amsterdam, 2002; Vol. *32*.
(15) Kimmich, R.; Anoardo, E. Field-Cycling NMR Relaxometry. *Prog. Nucl. Magn. Reson. Spectrosc.* **2004**, *44*, 257−320.
(16) Korb, J.-P.; Whaley-Hodges, M.; Bryant, R. G. Translational Diffusion of Liquids at Surfaces of Microporous Materials: Theoretical Analysis of Field-Cycling Magnetic Relaxation Measurements. *Phys. Rev. E* **1997**, *56*, 1934−1944.
(17) Godefroy, S.; Korb, J.-P.; Fleury, M.; Bryant, R. G. Surface Nuclear Magnetic Relaxation and Dynamics of Water and Oil in Macroporous Media. *Phys. Rev. E* **2001**, *64*, 021605−021612.
(18) Godefroy, S.; Fleury, M.; Deflandre, Korb, J.-P. Temperature on NMR Surface Relaxation in Rocks for Well Logging Applications. *J. Phys. Chem.* **2002**, *106*, 11183−11190.
(19) Korb, J.-P.; Freiman, G.; Nicot, B.; Ligneul, P. Dynamical Surface Affinity of Diphasic Liquids as a Probe of Wettability of Multimodal Porous Media. *Phys. Rev. E* **2009**, *80*, 061601−061612.
(20) Zielinski, L.; Hürlimann, M. D. Nuclear Magnetic Resonance Dispersion of Distributions as a Probe of Aggregation in Crude Oils. *Energy Fuels* **2011**, *2*, 5090−5099.
(21) Morris, K. F.; Johnson, C. S. Diffusion-Ordered Two-Dimensional Nuclear Magnetic Resonance Spectroscopy. *J. Am. Chem. Soc.* **1992**, *114*, 3139−3141.

(22) Johnson, C. S. Diffusion Ordered Nuclear Magnetic Resonance Spectroscopy: Principles and Applications. *Prog. Nucl. Magn. Reson. Spectrosc.* **1999**, *34*, 203−256.
(23) Butler, J. P.; Reeds, J. A.; Dawson, S. V. Estimating Solutions of First Kind Integral Equations with Non Negative Constraints and Optimal Smoothing. *SIAM J. Numer. Anal.* **1981**, *18*, 381−397.
(24) Venkataramanan, L.; Song, Y. Q.; Hürlimann, M. D. Solving Fredholm Integrals of the First Kind with Tensor Structure in 2 and 2.5 Dimensions. *IEEE Trans. Signal Process.* **2002**, *50*, 1017−1026.
(25) Bondino, I.; Nguyen, R.; Hamon, G.; Ormehaug, P. A.; Skauge, A.; Jouenne, S. In *Tertiary Polymer Flooding in Extra-Heavy Oil: An Investigation Using 1D and 2D Experiments, Core Scale Simulation and Pore-Scale Network Models*, International Symposium of the Society of Core Analysts, Austin, Texas, September 18−21, 2011; pp 1−12.
(26) Andrews, B. A.; Edwards, J. C.; Pomerantz, A. E.; Mullins, O. C.; Nordlund, D.; Norinaga, K. Comparison of Coal-Derived and Petroleum Asphaltenes by ^{13}C Nuclear Magnetic Resonance, DEPT, and XRS. *Energy Fuels* **2011**, *25*, 3068−3076.
(27) Acevedo, S.; Guzman, K.; Labrador, H.; Boutssiere, B. Trapping of Metallic Porphyrins by Asphaltene Aggregates: A Size Exclusion Microtomography with High-Resolution Inductively Coupled Plasma Mass Spectrometric Detection Study. *Energy Fuels* **2012**, *26*, 4968−4977.
(28) Sheu, E. Y. *Structures and Dynamics of Asphaltenes*; Mullins, O. C., Sheu, E. Y., Eds.; Plenum Press: New York, 1998; Chapter IV, pp 115−144.
(29) Benamsili, L.; Hamon G.; Korb, J.-P. Probing Individual Saturations of Crude-Oil/Brine/Mud-Filtrate Mixtures Confined in Rocks. In *Proceedings of MRPM11*, Guilford, U.K., September 2012, submitted to *Diffusion Fundamentals*.
(30) Lester, C.; Bryant, R. G. Water-Proton Nuclear Magnetic Relaxation in Heterogeneous Systems: Hydrated Lysozyme Results. *Magn. Reson. Med.* **1991**, *22*, 143−153.
(31) Barberon, F.; Korb, J.-P.; Petit, D.; Morin, V.; Bermejo, E. Probing the Surface Area of a Cement-Based Material by Nuclear Magnetic Relaxation Dispersion. *Phys. Rev. Lett.* **2003**, *90*, 1−4.
(32) Chang, C. L.; Fogler, H. S. Stabilization of Asphaltenes in Aliphatic Solvents using Alkyl Benzene Derived Amphiphiles, Part I. Effect of Chemical Structure of Amphiphiles on Asphaltene Stabilization. *Langmuir* **1994**, *10*, 1749−1757.
(33) Wang, J.; Buckley, J. S. Asphaltene Stability in Crude Oil and Aromatic Solvents-The Influence of Oil Composition. *Energy Fuels* **2003**, *17*, 1445−1451.
(34) Abragam, A. *The Principles of Nuclear Magnetism*; Clarendon: Oxford, U.K., 1961.
(35) Barbosa Guedes, C. L.; Di Mauro, E.; Antunes, V.; Mangrich, A. S. Photochemical Weathering Study of Brazilean Petroleum by EPR Spectroscopy. *Marine Chem.* **2003**, *84*, 105−112.
(36) Scotti, R.; Montanari, L. *Molecular Structure and Intermolecular Interaction of Asphaltenes by FT-IR, NMR, EPR, Structures and Dynamics of Asphaltenes*; Plenum: New York, 1998; Ch. 3, pp 79−113.
(37) Loskutova, Y. V.; Yudina, N. V.; Pisareva, S. I. Effect of Magnetic Field on the Paramagnetic, Antioxidant, and Viscosity Characteristics of Some Crude Oils. *Petroleum Chem.* **2008**, *48*, 51−55.
(38) Solomon, I. Relaxation Processes in a System of Two Spins. *Phys. Rev.* **1955**, *99*, 559−565.
(39) Bloembergen, N.; Morgan, O. Proton Relaxation Times in Paramagnetic Solutions Effects of Electron Spin Relaxation. *J. Chem. Phys.* **1961**, *34*, 842−850.
(40) Mutina, A. R.; Hürlimann, M. D. Effect of Oxygen on the NMR Relaxation Properties of Crude Oils. *Appl. Magn. Reson.* **2005**, *29*, 503−513.